Functional communication between IP_3R and STIM2 at subthreshold stimuli is a critical checkpoint for initiation of SOCE

Moaz Ahmad[a], Hwei Ling Ong[a,1], Hassan Saadi[a,1], Ga-Yeon Son[a,2], Zahra Shokatian[a,2], Lara E. Terry[b], Mohamed Trebak[c], David I. Yule[b], and Indu Ambudkar[a,3]

[a]Secretory Physiology Section, National Institute of Dental and Craniofacial Research, NIH, Bethesda, MD 20892; [b]Department of Pharmacology and Physiology, University of Rochester, Rochester, NY 14526; and [c]Department of Pharmacology and Chemical Biology, Vascular Medicine Institute, University of Pittsburgh School of Medicine, Pittsburgh, PA 15261

Edited by Mark Nelson, Pharmacology, University of Vermont, Burlington, VT; received August 20, 2021; accepted November 19, 2021

Stromal interaction molecules, STIM1 and STIM2, sense decreases in the endoplasmic reticulum (ER) $[Ca^{2+}]$ ($[Ca^{2+}]_{ER}$) and cluster in ER–plasma membrane (ER–PM) junctions where they recruit and activate Orai1. While STIM1 responds when $[Ca^{2+}]_{ER}$ is relatively low, STIM2 displays constitutive clustering in the junctions and is suggested to regulate basal Ca^{2+} entry. The cellular cues that determine STIM2 clustering under basal conditions is not known. By using gene editing to fluorescently tag endogenous STIM2, we report that endogenous STIM2 is constitutively localized in mobile and immobile clusters. The latter associate with ER–PM junctions and recruit Orai1 under basal conditions. Agonist stimulation increases immobile STIM2 clusters, which coordinate recruitment of Orai1 and STIM1 to the junctions. Extended synaptotagmin (E-Syt)2/3 are required for forming the ER–PM junctions, but are not sufficient for STIM2 clustering. Importantly, inositol 1,4,5-trisphosphate receptor (IP_3R) function and local $[Ca^{2+}]_{ER}$ are the main drivers of immobile STIM2 clusters. Enhancing, or decreasing, IP_3R function at ambient $[IP_3]$ causes corresponding increase, or attenuation, of immobile STIM2 clusters. We show that immobile STIM2 clusters denote decreases in local $[Ca^{2+}]_{ER}$ mediated by IP_3R that is sensed by the STIM2 N terminus. Finally, under basal conditions, ambient PIP_2-PLC activity of the cell determines IP_3R function, immobilization of STIM2, and basal Ca^{2+} entry while agonist stimulation augments these processes. Together, our findings reveal that immobilization of STIM2 clusters within ER–PM junctions, a first response to ER-Ca^{2+} store depletion, is facilitated by the juxtaposition of IP_3R and marks a checkpoint for initiation of Ca^{2+} entry.

STIM2 | IP3R | ER–PM junction | clustering | endogenous protein

Store-operated calcium entry (SOCE), which provides critical cytosolic Ca^{2+} signals for regulation of cell functions, is activated in response to depletion of Ca^{2+} stores within the endoplasmic reticulum (ER) (1, 2). Decreases in $[Ca^{2+}]_{ER}$ are sensed by resident ER proteins Stromal Interaction Molecules 1 and 2 (STIM1 and STIM2) via their luminal N-terminal Ca^{2+}-binding domains. This triggers their clustering in ER–plasma membrane (PM) junctions (3–5) where they recruit and activate the PM channel Orai1 (6–10). STIM1, the primary regulator of Orai1, has a relatively high Ca^{2+} affinity and responds to substantial decreases in $[Ca^{2+}]_{ER}$. In contrast, STIM2, a relatively weak activator of Orai1, has a lower Ca^{2+} affinity and can thus respond to minimal decreases in $[Ca^{2+}]_{ER}$ (4, 9–12). When overexpressed, STIM2 displays constitutive clustering within ER–PM junctions where it recruits and activates Orai1 channels to cause Ca^{2+} entry in unstimulated cells (4, 12, 13). We previously demonstrated that preclustering of STIM2 promotes recruitment of Orai1/STIM1 and facilitates STIM1 activation under conditions when $[Ca^{2+}]_{ER}$ is not sufficiently depleted to activate STIM1 (9, 10). These data suggest that preclustered STIM2 is in an activated state in unstimulated cells. There is, however, little information regarding the clustering of endogenous STIM2 and the molecular mechanisms, or cellular cues, that regulate its preclustering at ER–PM junctions in the cell. A particular concern is that exogenous overexpression of STIM2 alters the stoichiometry of endogenous STIM/Orai complexes, which might artificially force them into the junctions to cause preclustering.

We have used CRISPR/Cas9 to knockin mVenus into the N terminus of the native *Stim2* gene and generated HEK293 cell lines expressing fluorescently tagged endogenous STIM2 (mV-STIM2). Herein we report that endogenous STIM2 is preclustered in the ER–PM junctional region of cells under basal conditions. While the majority of STIM2 clusters are mobile, there is a small population of relatively immobile STIM2 clusters. Importantly, immobilization of native STIM2 clusters is triggered by decreases in local $[Ca^{2+}]_{ER}$ that are mediated by functional IP_3 receptors (IP_3R) and sensed by STIM2 N terminus. In the absence of added agonist, constitutive PIP_2-PLC activity, together with cAMP/protein kinase A (PKA) signaling, determines IP_3R function. Consistent with this response of STIM2 at ambient stimuli, there is an increase in immobile

Significance

STIM proteins sense decreases in $[Ca^{2+}]_{ER}$ and cluster in endoplasmic reticulum (ER)–plasma membrane (PM) junctions where they recruit and activate Orai1. While STIM1 clustering requires substantial $[Ca^{2+}]_{ER}$ decrease, STIM2 displays preclustering under resting conditions and regulates basal Ca^{2+} entry. The mechanism(s) underlying constitutive clustering of STIM2 is not known. We show herein that endogenous STIM2 assembles as mobile and immobile clusters and that Orai1 is recruited to the latter. Anchoring of STIM2 clusters is triggered by decreases in local $[Ca^{2+}]_{ER}$ that are mediated by ambient activity of IP_3R and sensed by the STIM2 N terminus. This functional link between IP_3R and STIM2 governs constitutive STIM2 clustering and ensures coupling of $[Ca^{2+}]_{ER}$ decrease at subthreshold stimuli with activation of Ca^{2+} entry.

Author contributions: M.A., H.L.O., M.T., D.I.Y., and I.A. designed research; M.A., H.L.O., H.S., G.-Y.S., Z.S., and L.E.T. performed research; M.A., H.L.O., H.S., L.E.T., M.T., D.I.Y., and I.A. contributed new reagents/analytic tools; M.A., H.L.O., H.S., G.-Y.S., Z.S., L.E.T., and I.A. analyzed data; and M.A., H.L.O., M.T., D.I.Y., and I.A. wrote the paper.

The authors declare no competing interest.

This article is a PNAS Direct Submission.

[1]H.L.O. and H.S. contributed equally to this work.

[2]Present address: New York University College of Dentistry, New York, NY 10010.

[3]To whom correspondence may be addressed. Email: indu.ambudkar@nih.gov.

This article contains supporting information online at http://www.pnas.org/lookup/suppl/doi:10.1073/pnas.2114928118/-/DCSupplemental.

Published January 12, 2022.

STIM2 clusters following simulation of cells with a Ca^{2+}-mobilizing agonist. Further, the immobile STIM2 clusters demarcate sites where Orai1 clusters in basal conditions and both Orai1 and STIM1 cluster following agonist stimulation. Together, our findings suggest that a critical functional link between IP_3R and STIM2 underlies preclustering of STIM2 and is a checkpoint for initiation of SOCE in response to decreases in $[Ca^{2+}]_{ER}$.

Results

Endogenous STIM2 Is Preclustered in ER–PM Junctions. mVenus was knocked in at the N terminus of the *Stim2* gene using the CRISPR/Cas9 approach in HEK293 cells (experimental details are provided in *SI Appendix*, Fig. S1 *A* and *B*) and integration of mVenus was confirmed by PCR and genomic sequencing. HEK293 cells expressing mVenus-STIM2 (mV-STIM2, indicated as S2 in all the figures) were isolated by single-cell sorting (*SI Appendix*, Fig. S1 *C* and *D*) and used to establish a monoclonal cell population (STIM2-KI cells, which were used for all the experiments described below unless indicated otherwise). All STIM2-KI cells expressed mV-STIM2, which was substantially reduced by siSTIM2 (*SI Appendix*, Fig. S1*E*). STIM2 expression was similar in wild-type (WT) HEK293 and STIM2-KI cells; note the presence of mV-STIM2 in the latter (*SI Appendix*, Fig. S1*F*). Further, expressions of STIM1 and Orai1, as well as cyclopiazonic acid (CPA)-induced internal Ca^{2+} release and Ca^{2+} entry, were similar in WT and STIM2-KI cells (*SI Appendix*, Fig. S1 *G–J*). Also, knockdown of either STIM protein expression significantly reduced Ca^{2+} influx, with relatively greater decrease induced by STIM1 knockdown.

mV-STIM2 displayed a reticular pattern of localization in STIM2-KI cells (Fig. 1*A*, confocal image; an enlarged view shown on the *Right*). mV-STIM2 colocalized with an ER marker (mCherry-ER3, mCh-ER3) in STIM2-KI cells (Fig. 1*B*), although mV-STIM2 signal was not uniform in the ER but rather displayed a punctate pattern (Pearson's correlation coefficient [PCC] = 0.76 and Mander's overlay coefficient [MOC] = 0.98/0.98). mV-STIM2 was detected as clusters in the total internal reflection fluorescence (TIRF) plane in unstimulated cells (Fig. 1*C*) as was mCh-ER3 (expressed in WT HEK293 cells, Fig. 1*D*). mV-STIM2 was localized within this ER network in STIM2-KI cells expressing mCh-ER3 (Fig. 1*E*, enlarged area shown in Fig. 1*F*, also see line scans; PCC = 0.57 and MOC = 0.99/0.97). Although not all areas of the ER had STIM2, every STIM2 cluster was colocalized with the ER. More mV-STIM2 clusters were recruited to ER–PM junctions, without ER-Ca^{2+} store depletion, when MAPPER (14) was expressed in STIM2-KI cells (mV-STIM2 was colocalized with mCerulean-MAPPER (mC-MAPPER), PCC = 0.75 and MOC M1/M2 = 0.89/0.97; line scans show overlapping peaks of both proteins) (Fig. 1*G*).

Endogenous STIM2 Exists as Immobile and Mobile Clusters. Stimulation of STIM2-KI cells with relatively low (1 μM) or high (100 μM) carbachol (CCh), caused a time- and dose-dependent increase in the number and fluorescence intensity of mV-STIM2 clusters (Fig. 2 *A* and *B*, addition of the agonist at 2 min is indicated; Movies S1 and S2). Activation-induced clustering of STIM1 and Orai1 in ER–PM junctions is associated with a decrease in their mobility (15). Since STIM2 is suggested to be in an activated state under basal conditions, we examined the mobility of mV-STIM2 in unstimulated cells by identifying those that remained at the same location for at least 1 min (similar criteria have been previously used to determine stability of proteins, including IP_3R) (16). A small proportion of mV-STIM2 clusters was relatively immobile under ambient conditions (Fig. 2 *C* and *D* show enlarged areas of STIM2-KI cells; whole cell image is shown in *SI Appendix*, Fig. S2). The images in Fig. 2 *C* and *D* labeled as "basal" show mV-STIM2 clusters (green) present in the first frame (indicated as 0) overlaid with the image acquired 1 min later (0/1m; mV-STIM2 clusters in second frame are indicated in magenta). Clusters that overlap (white) represent those that remained at the same location for 1 min (also shown by line scans to the *Right* of the image). Note that relatively immobile clusters displayed similar location and fluorescence amplitude in subsequent frames, while mobile clusters appeared as nonoverlapping magenta and green peaks with different amplitudes. Importantly, the number of these immobile clusters was increased dose dependently following stimulation of the cells with low (1 μM) or high (100 μM) CCh (Fig. 2 *C* and *D*, appear as white clusters in the images and as overlapping peaks in the line scans). Cells were stimulated at the 2-min time point, and overlay images from 3 and 4 min (3/4m; i.e., 1 and 2 min after stimulation) were used to identify early changes in mobility of mV-STIM2 clusters. Time-dependent changes in immobile mV-STIM2 clusters were quantified (Fig. 2*E*). The increase in immobile mV-STIM2 clusters (relative to the number of immobile clusters at 2 min, i.e., prior to stimulation) was higher at 100 μM than 1 μM CCh (also reflected by the increase in PCC values) (Fig. 2*F*).

The response of Orai1 to agonist stimulation in STIM2-KI cells was determined by expressing the proteins using the relatively weak thymidine kinase (TK) promoter, to limit the amount of expressed protein (17). While TK-Orai1-CFP (TK-O1) displayed a diffuse localization at the TIRF plane both in HEK293 cells (*SI Appendix*, Fig. S3*A*) and S2KI-HEK293 cells (*SI Appendix*, Fig. S3*B*), a few channel clusters could be seen prior to stimulation in both sets of cells (basal condition image and *SI Appendix*, Fig. S3 *A* and *B*). These TK-O1 clusters displayed overlap with mV-STIM2 clusters in basal STIM2-KI cells (*SI Appendix*, Fig. S3*B*, *Upper* images) and increased after stimulation with 1 μM CCh (*SI Appendix*, Fig. S3*A*, *Upper Right* image) together with coclustering of both proteins (*SI Appendix*, Fig. S3*B*, *Lower* images and line scan). Note that immobile TK-O1 clusters were detected in STIM2-KI cells prior to stimulation (*SI Appendix*, Fig. S3*C*, white clusters; tracking was done for a minute, 0/1m as described for Fig. 2), which increased following CCh stimulation (*SI Appendix*, Fig. S3*D* shows overlay of TK-O1 signal 1 and 2 min after stimulation, frames 3/4m). *SI Appendix*, Fig. S3 *E* and *F* show mV-STIM2 in the same cell. Fig. 2*G* shows recruitment of Orai1 to immobile STIM2 clusters (in this case, STIM2 clusters that were not preclustered with TK-O1 were tracked). (*i* and *ii*) A single STIM2 cluster that remained at the same location for a minute after 1 μM CCh stimulation (white cluster in second image indicates that it is immobile). (*iii*) Orai1 cluster was not detected prior to stimulation but seen at the same location as the mV-STIM2 cluster by 1 min after stimulation, staying at that location for another minute. (*iv* and *v*) Increase in number of immobile clusters containing TK-O1 and mV-STIM2 after 1 μM CCh stimulation (Fig. 2*H*). Orai1 clustering in resting and stimulated cells was abrogated by silencing STIM2 (*SI Appendix*, Fig. S3*A*, *Lower* images). TK-O1 clusters were also seen in unstimulated WT cells with increase after stimulation with 1 μM CCh (*SI Appendix*, Fig. S3*H*). It is likely that the relatively low abundance of expressed Orai1 in the present study allowed detection of Orai1 clusters in resting cells.

TK-mCh-STIM1 (TK-S1), expressed in STIM2-KI cells, displayed the characteristic tracking pattern in cells under basal condition (*SI Appendix*, Fig. S4 *A* and *B*, *Upper* images). TK-S1 (red) was not clustered with mV-STIM2 clusters (green) in basal cells (*SI Appendix*, Fig. S4*A*) but coclustered 5 min after 1 μM CCh stimulation. TK-S1 clustering at 1 μM CCh (images on the *Right*), but not at 100 μM CCh stimulation (*Lower* images), was dependent on endogenous STIM2 (*SI Appendix*, Fig. S4*B*). In contrast, basal clustering of mV-STIM2 and the

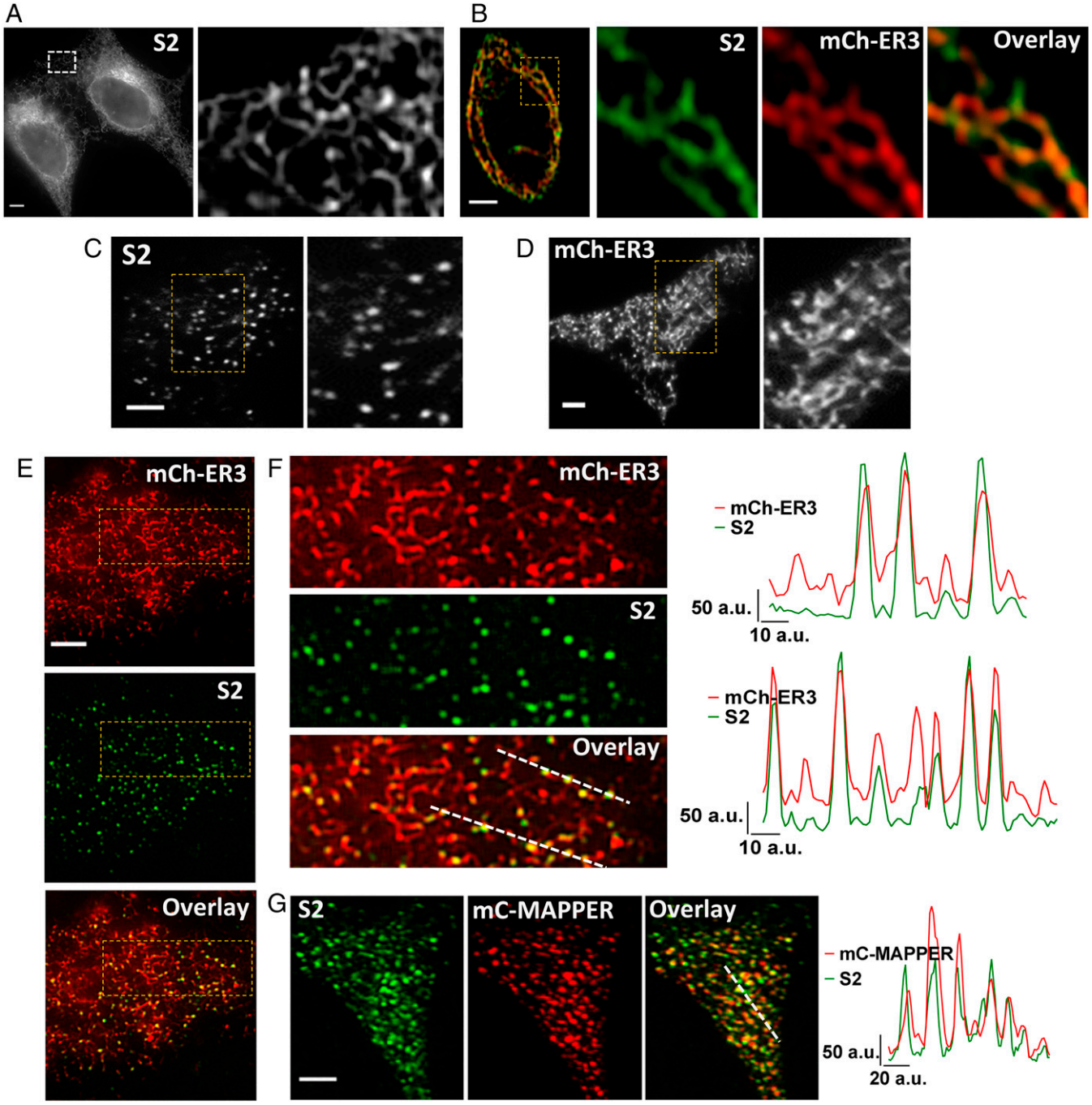

Fig. 1. Visualization of endogenous STIM2. (*A*) Localization of endogenous mVenus-STIM2 (mV-STIM2; S2 in images, acquired by confocal microscopy) in STIM2-KI cells, enlargement of the demarcated area shown on the *Right*. (*B*) Airyscan images with enlarged region of STIM2-KI cell showing mV-STIM2 (green), expressed mCherry-ER3 (mCh-ER3, red), and overlay. (*C*) TIRFM images of STIM2-KI cells in basal, unstimulated conditions with enlargement of demarcated area on the *Right*. (*D*) Localization of mCh-ER3 in HEK293 with enlarged area on the *Right*. (*E*) Images from *Upper* to *Lower*: mCh-ER3 expressed in STIM2-KI cells (ER, red), mV-STIM2 (S2, green), and overlay. (*F*) Enlarged images of demarcated regions in *E* and line scans (position indicated in overlay image mCh-ER3 [ER, red] and mVenus-STIM2 [S2, green]). (*G*) mCerulean-MAPPER (mC-MAPPER, pseudocolored red) expressed in STIM2-KI cells and mV-STIM2 (S2, green), and overlay; line scans (position indicated in overlay image) show mC-MAPPER (red) and mV-STIM2 (green). All microscope images show representative cells from at least three experiments. (Scale bars, 5 μm.) a.u.: arbitrary units.

increase after 1 μM CCh was not dependent on endogenous STIM1 (*SI Appendix*, Fig. S4*C*). While some TK-S1 clusters were seen before CCh stimulation (*SI Appendix*, Fig. S4*D*), a few immobile TK-S1 clusters detected 1 and 2 min after stimulation (*SI Appendix*, Fig. S4*E*, overlay of frames 3/4m, mV-STIM2 clusters shown in *SI Appendix*, Fig. S4*F*) with an increase in immobile clusters by 4 to 5 min of stimulation (*SI Appendix*, Fig. S4*G*, overlay of frames 6/7m, mV-STIM2 shown in *SI Appendix*, Fig. S4*H*). Fig. 2*I* shows that STIM2 clusters (*i*) that were identified as stable (*ii*; overlap of clusters between 2 and 3 min after stimulation, 4/5m) marked the site where TK-S1 coclustered after stimulation (indicated by white arrows). TK-S1 clusters were detected at these locations only 2 min after stimulation (*v*), but not at earlier time points

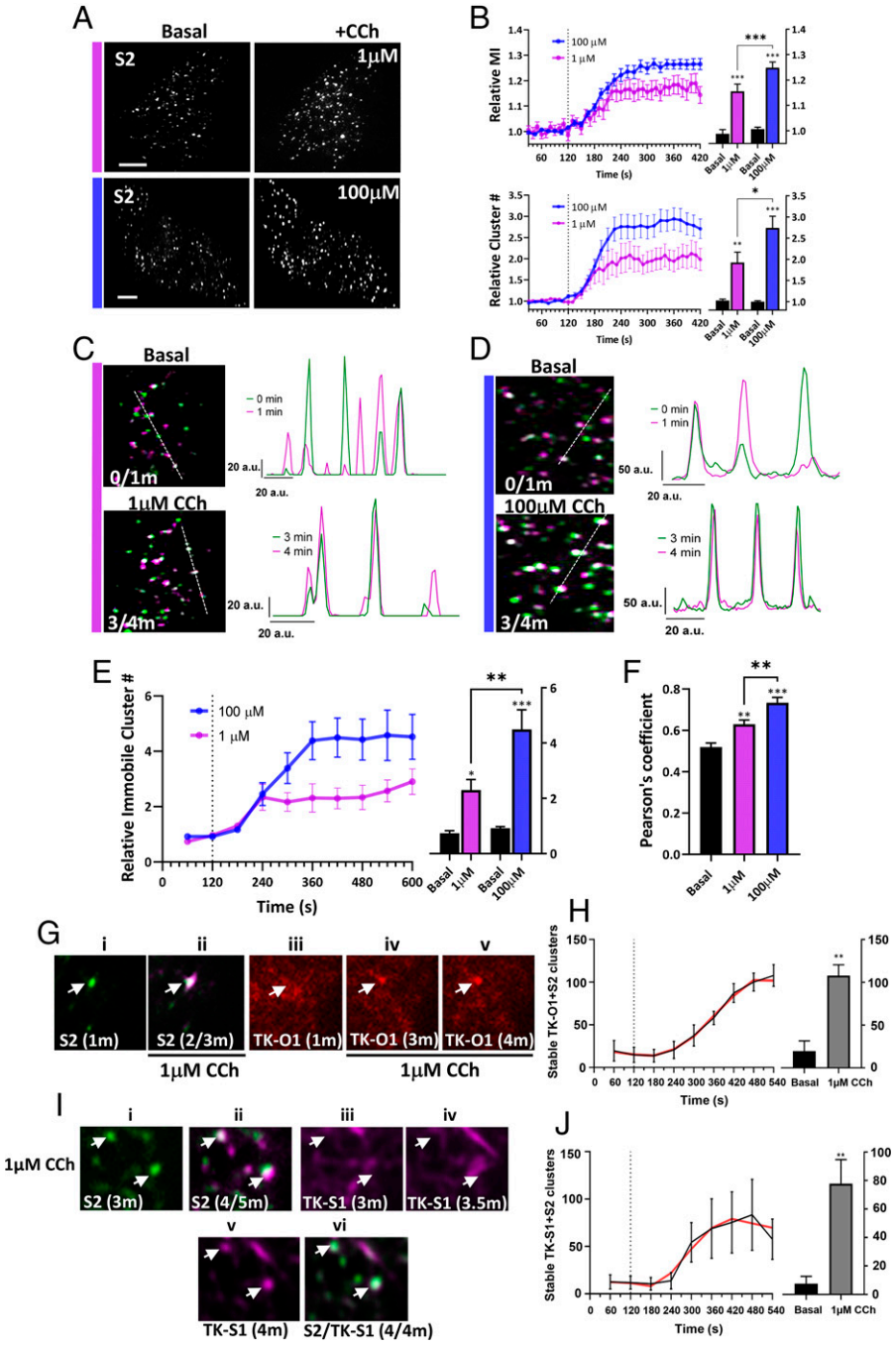

Fig. 2. mVenus-STIM2 clusters display decreased mobility in response to carbachol stimulation. (*A*) mV-STIM2 in STIM2-KI cells (S2 in images) before (*Left*) and after (*Right*) stimulation (with 1 μM or 100 μM CCh). (*B*) mV-STIM2 cluster intensity (mean ± SEM of mean intensity [MI], *Upper*) and number (cluster #, *Lower*) in response to 1 μM (magenta) or 100 μM CCh (blue) (dotted line indicates CCh addition). Bar graphs showing values at 1-min (basal) and 5-min (stimulated; 1 μM or 100 μM) time points. (*C*) Overlay of mV-STIM2 images taken at 1-min intervals (clusters pseudocolored either magenta or green) with immobile clusters appearing as white. The overlay images before stimulation (frames 0- and 1-min time points, 0/1m; *Upper*) and after stimulation with 1 μM CCh (3- and 4-min time points, 3/4m). Line scans are on the *Right* (position indicated in overlay images). (*D*) Images were analyzed as described in *C* for cells before and after stimulation with 100 μM CCh. (*E*) Increase of immobile mV-STIM2 (mean ± SEM) clusters stimulated with 1 μM (magenta) or 100 μM CCh (blue). Bar graphs (*Right*) showing number of clusters before and after stimulation. (*F*) Pearson's correlation coefficients of clusters in *C* and *D*, basal and after stimulation (1 and 5 min). (*G*) TK-O1 recruitment to immobile S2 clusters. S2 cluster (*i*) prior to stimulation (1 min) and (*ii*) overlay of S2 after stimulation with 1 μM CCh (2/3 min overlay, immobile cluster indicated by arrow). TK-O1 cluster (*iii*) prior to stimulation and following stimulation at the (*iv*) 3- and (*v*) 4-min time points, with the emergent cluster colocalized with the stable mV-STIM2 cluster (arrow). (*H*) Increase in immobile clusters containing both TK-O1 and S2 after 1 μM CCh addition; bar graph showing number of stable clusters before (basal) and after CCh stimulation (1- and 9-min time points, respectively, smoothened curve in red). (*I*) TK-S1 recruitment to immobile S2 clusters. S2 clusters at (*i*) 3 min, (*ii*) overlay of images from 4- and 5-min (4/5m overlay) time points. TK-S1 clusters after CCh stimulation at (*iii*) 3-, (*iv*) 3.5-, and (*v*) 4-min time points. (*vi*) Overlay of TK-S1 and S2 at 4-min time point (4/4m). (*J*) Increase in immobile clusters containing both TK-S1 and S2 after 1 μM CCh stimulation; bar graph showing number of stable clusters before (basal) and after CCh stimulation (1- and 9-min time points respectively, smoothened curve [red]). All images were acquired using TIRFM and are representative of cells from at least three experiments with CCh added at 2 min. Statistical significance was assessed using Student's *t* tests for two groups and ANOVA for multiple groups, and presented as $*P < 0.05$, $**P < 0.01$, and $***P < 0.001$. (Scale bars, 5 μm.) a.u.: arbitrary units.

(*iii* and *iv* show images at 1 and 1.5 min after stimulation). The final panel (*vi*) shows colocalization of stable STIM2 clusters overlapping with a newly formed STIM1 cluster (marked by white arrows). Time-dependent increase in number of immobile clusters containing both mV-STIM2 and TK-S1 following stimulation of cells with 1 μM CCh is shown in Fig. 2*J*.

E-Syts2/3-Dependent ER–PM Junctions Mark the Site of Endogenous STIM2 Clustering. Extended synaptotagmins 2 and 3 (E-Syts2/3) serve as constitutive tethers linking the ER with the PM (18). Simultaneous knockdown of E-Syts2/3 expression in STIM2-KI cells greatly reduced mV-STIM2 clusters in resting cells (Fig. 3*A*) while overexpression of either protein increased mV-STIM2 clusters in unstimulated cells (Fig. 3 *B* and *C*). Localization of the ER, or constitutive clusters of MAPPER, were not dependent on endogenous STIM2 but were attenuated by loss of E-Syts2/3 expression (Fig. 3 *D* and *E*, respectively). Stable preformed junctions, indicated by immobile mC-MAPPER clusters were also reduced (Fig. 3*F*). Knockdown of E-Syt2 or E-Syt3 expression by siE-Syts2/3 siRNA is shown in *SI Appendix*, Fig. S4 *I* and *J*.

The increase in coclustering of mV-STIM2 and TK-O1 following stimulation with 1 μM CCh was substantially decreased in cells with knockdown of E-Syts2/3 (Fig. 3*G*, *i*, *ii*, and *iii* and Movie S3), although there was some recovery of clustering following stimulation with 100 μM CCh (Fig. 3*G*, *i*, *ii*, and *iv*). Similar effects were seen for coclustering of TK-STIM1 and mV-STIM2 in response to stimulation with 1 and 100 μM CCh (Fig. 3*H*). Consistent with the effect of E-Syts2/3 knockdown on protein clustering, siE-Syts2/3 reduced Ca^{2+} entry stimulated by low but not high [CCh] (Fig. 3*I*, Ca^{2+} release was not affected). These data suggest that E-Syts2/3-mediated ER–PM tethering is required for STIM2 preclustering in the ER–PM junctional region in basal conditions and following low-intensity stimulation. Other tethering proteins, e.g., E-Syt1, might have a greater contribution to ER–PM junction assembly and STIM/Orai1 clustering at high-stimulus intensities (18–20).

Mobility of STIM2 Clusters Is Dependent on IP_3R. To examine the contribution of other cellular cues, such as decrease in local $[Ca^{2+}]_{ER}$, to mV-STIM2 clustering, IP_3R1-mCherry was expressed in STIM2-KI cells. Both proteins clustered in the ER–PM junctional region of unstimulated cells (Fig. 4*A*, line scans), with partial overlap between their clusters (Pearson's coefficient was 0.625 ± 0.06). Immobile mV-STIM2 clusters (Fig. 4*B*, *Upper* images and line scan) and immobile IP_3R1 clusters (Fig. 4*B*, *Lower* images and line scan) were detected in the same cellular location and displayed partial overlap (magnified image after 1 μM CCh is shown in Fig. 4*C*; note that images in Fig. 4 *A*–*C* were acquired from the same cell). Importantly, clustering of mV-STIM2 was strongly attenuated by knockdown of IP_3Rs both in unstimulated cells and after 1-μM CCh stimulation (Fig. 4*D* and Movie S4) as was the time-dependent increase in mV-STIM2 clusters following 1-μM CCh stimulation (Fig. 4*E*). The presence of the ER (indicated by mCh-ER3 signal in Fig. 4*F*) in the TIRF plane was not affected by knockdown of IP_3Rs. Knockdown of E-Syts2/3, which disrupted localization of ER in the subplasma membrane region, abrogated the clustering of IP_3R1-mCherry (Fig. 4*G*) and reduced immobile clusters of STIM2, similar to that induced by siIP_3R (Fig. 4*H*, respectively).

Mobility of STIM2 Clusters Is Determined by IP_3R Function and Decrease of Local $[Ca^{2+}]_{ER}$. Coimmunoprecipitation (co-IP) experiments revealed that neither Myc-tagged STIM1 nor STIM2 were pulled down together with IP_3R1 (*SI Appendix*, Fig. S5*A*, reverse co-IP shown in *SI Appendix*, Fig. S5*B*). The involvement of IP_3R function in constitutive clustering of STIM2 was assessed by treating STIM2-KI cells with forskolin (FSK) that allosterically enhances IP_3R channel activity via PKA-dependent phosphorylation in the absence of an increase in $[IP_3]$ or IP_3 binding (21, 22). FSK (5 μM) addition to STIM2-KI cells increased the number and mean fluorescence intensity of mV-STIM2 clusters (Fig. 5, *Upper* two images in *A* and graph in B; Movie S5) and the number of immobile mV-STIM2 clusters (*Lower* images in Fig. 5*A* show overlap of images acquired prior to [basal, 0/1m] and after FSK addition [3/4m]). Fig. 5*C* shows FSK-induced time-dependent increase in the number of mV-STIM2 clusters. Similar results were obtained when TK-STIM2 was expressed in WT HEK293 cells (Fig. 5*D*). Further, constitutive and FSK-induced STIM2 clustering was attenuated in cells lacking all three IP_3Rs (IP_3R-TKO) that were treated with siE-Syts2/3, although CPA treatment restored STIM2 clustering (Fig. 5*E*, also see bar graphs).

ER-LAR-GECO1 was used to measure $[Ca^{2+}]_{ER}$ at the TIRF plane of STIM2-KI cells. Fig. 5*F* shows images of mV-STIM2 (*Upper* set) and ER-LAR-GECO (*Lower* set) in basal and FSK-treated STIM2-KI cells. Immobile STIM2 clusters were identified (squares). Regions of interest (ROI) measurements of individual immobile STIM2 puncta showed an increase in mV-STIM2 intensity concident with a decrease in ER-LAR-GECO1 intensity following FSK treatment (enlarged images in Fig. 5*F* and graph in Fig. 5*G*; time course of the decrease is shown in Fig. 5*H*). FSK did not induce any change in ER-LAR-GECO1 fluorescence in IP_3R-TKO cells. The decrease in ER-LAR-GECO1 fluorescence seen in FSK-treated WT cells was comparable to that in STIM2-KI cells (Fig. 5*H* and *SI Appendix*, Fig. S5 *C*–*E*).

Determinants of IP_3R Function and STIM2 Preclustering in Resting Cells. The role of IP_3Rs in STIM2 clustering was further studied by expressing TK-YFP-STIM2 construct (TK-S2) in WT HEK293 cells or IP_3R-TKO (23), IP_3R-TKO stably expressing WT-IP_3R1 (IP_3R1), a pore dead mutant of IP_3R1 ($IP_3R1G2506R$) (24), or a phosphorylation-deficient mutant of IP_3R1 (IP_3R1-S1589A/S1755A, Phos-mutant) (25). In WT cells, TK-YFP-STIM2 displayed constitutive clusters, which were increased by FSK addition and further increased by CPA (Fig. 6*A*, first column; Movie S6). In the IP_3R-TKO cells, constitutive TK-YFP-STIM2 clustering was reduced and there was no increase after FSK addition, although subsequent addition of 25 μM CPA induced clustering (Fig. 6*A*, second column and Movie S7). Constitutive clustering of TK-YFP-STIM2 was also reduced in IP_3R-TKO cells expressing the pore-deficient IP_3R1/G2506R or phosphoryation-deficient IP_3R1. Further, FSK did not increase STIM2 clustering while subsequent addition of CPA did (Fig. 6*A*, third and fourth columns). Constitutive clustering of TK-YFP-STIM2 and FSK enhancement of clusters were restored in IP_3R-TKO cells stably expressing wild-type IP_3R1 (Fig. 6*A*, last column and Movie S8). The relative increase in TK-S2 clusters (number and mean fluorescence intensity) seen in WT cells after FSK addition was significantly attenuated in IP_3R-TKO cells or cells expressing mutant IP_3Rs but was rescued in cells expressing IP_3R1 (Fig. 6*B*). Time-dependent changes in STIM2 clustering following FSK stimulation in the different sets of cells are shown in Fig. 6 *C* and *D*, while Fig. 6*E* shows the effect of IP_3R function on STIM2 cluster size in basal conditions and after FSK stimulation.

The role of ambient PIP_2-PLC activity was determined by treating WT HEK293 cells expressing TK-YFP-STIM2 with the PLC inhibitor, U73122. This compound, but not the inactive analog, U73343, decreased STIM2 preclustering as well as FSK-induced enhancement of clustering (Fig. 6 *F* and *G*). These results support previous reports demonstrating PKA-dependent phosphorylation enhances IP_3R function at low levels of IP_3 (21). Additionally, the PKA inhibitor, H89, also suppressed FSK-induced increase in TK-YFP-STIM2 clustering (see images and bar graphs in Fig. 6 *H* and *I*). Importantly, constitutive clustering

PHYSIOLOGY

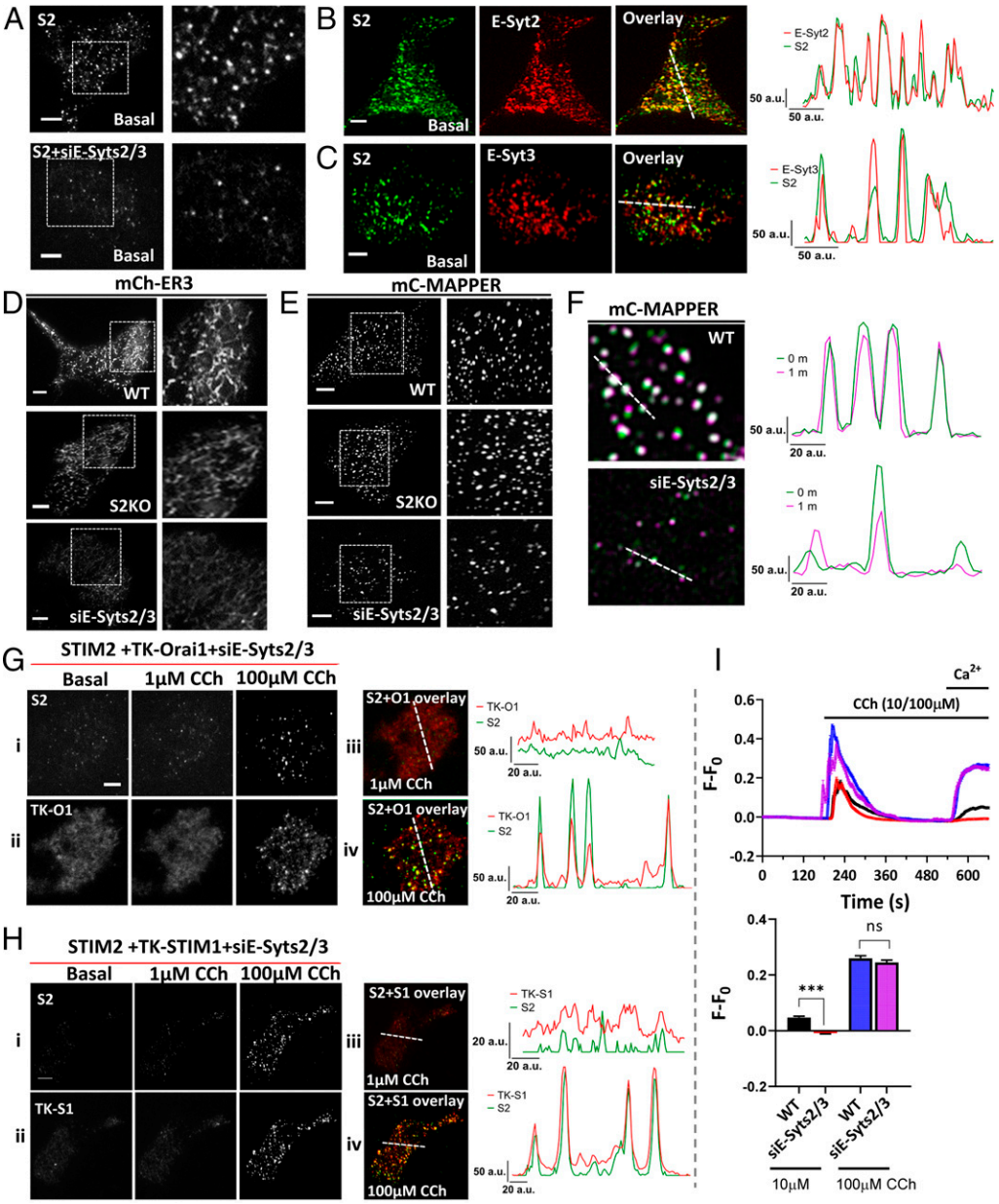

Fig. 3. Role of extended synaptotagmins in localization of mVenus-STIM2 in ER–PM junction. (*A*) mV-STIM2 (S2) in control (*Top*) and siE-Syts2/3-transfected STIM2-KI cells (*Bottom*); enlargement of demarcated area on the *Right*. (*B* and *C*) Unstimulated STIM2-KI cells expressing (*B*) mCh-E-Syt2 (E-Syt2) or (*C*) mCh-E-Syt3 (E-Syt3). From *Left* to *Right*: S2 (green), E-Syt2 or E-Syt3 (red), and overlay of both proteins (colocalized clusters in yellow). Line scans (position indicated in overlay image) show overlapping mV-S2 and E-Syt clusters. (*D*) mCherry-ER3 (mCh-ER) or (*E*) mC-MAPPER expressed in WT (*Top*) or STIM2 knockout (S2KO, *Middle*) HEK293 cells, and WT cells treated with siE-Syts2/3 (*Bottom*). Enlargements of the area demarcated by a square box are shown on the *Right*. (*F*) Overlay images of mCerulean-MAPPER in WT cells (*Top*) and WT cells treated with siE-Syts2/3 (*Bottom*) under basal/unstimulated conditions (0/1m overlay) where white clusters represent immobile clusters. Line scans (position indicated in overlay image) show overlapping peaks for relatively immobile clusters. (*G*) STIM2-KI cells transfected with siE-Syts2/3 in addition to TK-Orai1-mCh; (*i*) mVenus-STIM2 (S2) and (*ii*) TK-Orai1-mCh (TK-O1) in unstimulated (*Left*), 1 μM CCh (*Middle*), and 100 μM conditions (*Right*). (*iii* and *iv*) Overlay of mV-STIM2 (S2, green) and TK-Orai1-mCh (TK-O1, red) following stimulation with 1 μM and 100 μM CCh, respectively. Line scans (position indicated on the overlay images) showing colocalized clusters of S2 and TK-O1. (*H*) Similar set of experiments as in *G* but with STIM2-KI cells expressing TK-mCh-STIM1 (TK-S1) + siE-Syts2/3. (*I*) Fura-2 fluorescence ($F\text{-}F_0$, mean ± SEM) in control WT and siE-Syts2/3-treated WT cells stimulated with 10 μM or 100 μM CCh. Bar graphs show increase in fluorescence due to 1 mM Ca^{2+} entry. All TIRFM images show representative cells from at least three experiments, with CCh added at the 2-min time point. The Ca^{2+} imaging data are based on $n > 150$ cells in each set. Statistical significance was assessed using Student's *t* tests for two groups and presented as not significant (ns: $P = 0.4$) and significant (***$P < 0.001$). a.u.: arbitrary units.

of STIM2 in the ER–PM junctional region was reduced by H89 treatment. Consistent with this, basal Ca^{2+} entry was significantly decreased by treatment with PLC or PKA inhibitors and by knockdown of endogenous STIM2 (Fig. 6 *J* and *K*). Interestingly, consistent with enhancement of mV-STIM2 clustering in ER–PM junctions by MAPPER expression (Fig. 1*G*), constitutive Ca^{2+} entry was faster and abrogated by knockdown of endogenous STIM2 (*SI Appendix*, Fig. S5*F*). It is important to note that the contribution of cAMP/PKA to STIM2 preclustering in resting cells is likely to vary among different cell types. HEK293 cells have relatively high constitutive cAMP/PKA activity (26) and thus H89 was effective in reducing STIM2

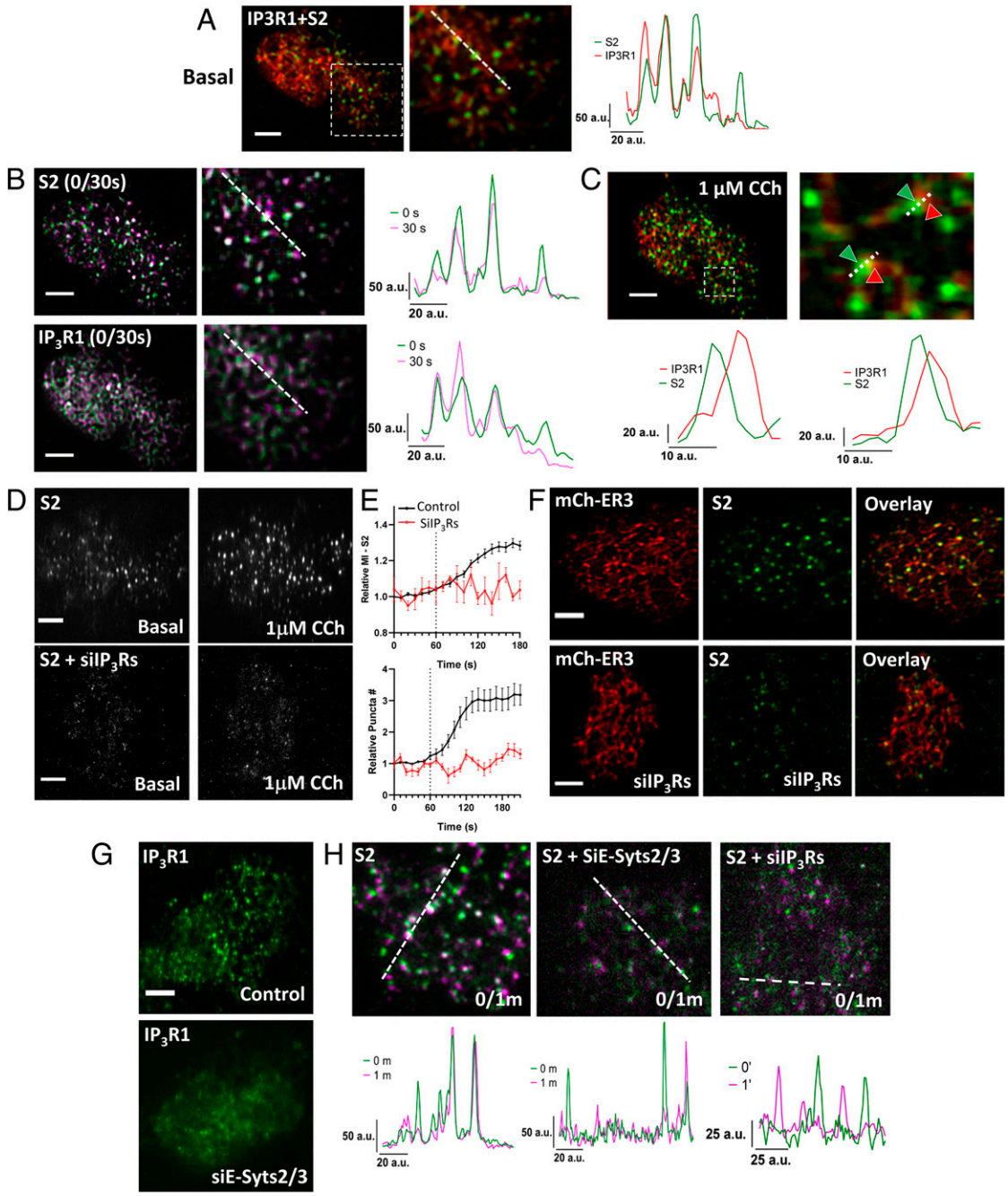

Fig. 4. Clustering of STIM2 in the ER–PM junctional region depends on IP_3Rs. (*A*) Overlay of mV-STIM2 (S2, green) and IP_3R1-mCherry (IP3R1, red; expressed in STIM2-KI cells) with an enlarged image of demarcated area and line scan (position indicated on the enlarged overlay image). (*B*) Overlay images of S2 (*Top*) and IP_3R1-mCherry (IP_3R1, *Bottom*) from 0-and 30-s time points and line scans (position indicated on the enlarged overlay image). (*C*) Same cell as in *A* and *B* stimulated with 1 μM CCh: overlay image of IP_3R1 (red) and S2 (green) clusters and enlarged area (*Right*). Line scan (*Below*) shows positions of the two proteins in two clusters (indicated by arrows). (*D*) STIM2-KI cells showing S2 (*Top*) or cells with knockdown of all IP_3R isoforms (*Bottom*). In each case, S2 fluorescence in unstimulated and 1 μM CCh-stimulated cells are shown. (*E*) Increase in S2 cluster (mean intensity [*Top*] and relative cluster number [*Bottom*] in control [black trace] and IP_3Rs knockdown cells [red trace]). (*F*) STIM2-KI cells expressing mCherry-ER3 showing S2 (green) and mCherry-ER3 (ER, red) in control (*Top*) and $siIP_3Rs$-treated (*Bottom*) without stimulation. (*G*) Wild-type HEK293 transfected with IP_3R1 or IP_3R1 + siE-Syts2/3. (*H*) Overlay images of S2 clusters in STIM2-KI cells alone or with si-Esyt2/3 or $siIP_3Rs$ treatment from 0- and 1-min time points (0/1m). Line scan shows overlapping peaks of both time points under basal condition. All TIRFM images show representative cells from at least three experiments. (Scale bars, 5 μm.) a.u.: arbitrary units.

preclustering in unstimulated cells. Other factors, such as the metabolic status (i.e., amount of adenosine triphosphate) that allosterically increase IP_3R activity via enhancing the sensitivity of the receptor to IP_3, could also act in a manner similar to PKA (27). We also cannot rule out a role for IP_3R binding partners that enhance activity in the preclustering (28).

STIM2 N Terminus Determines Immobilization of STIM2 Clusters in Unstimulated Cells. A STIM2 chimera where the N terminus was replaced with that of STIM1 (S1N-S2C) and a STIM1 chimera containing STIM2 N-terminal domain (S2N-S1C) were used to determine whether STIM2 N-terminal EF-hand domain senses local $[Ca^{2+}]_{ER}$ calcium decrease under ambient conditions. TK

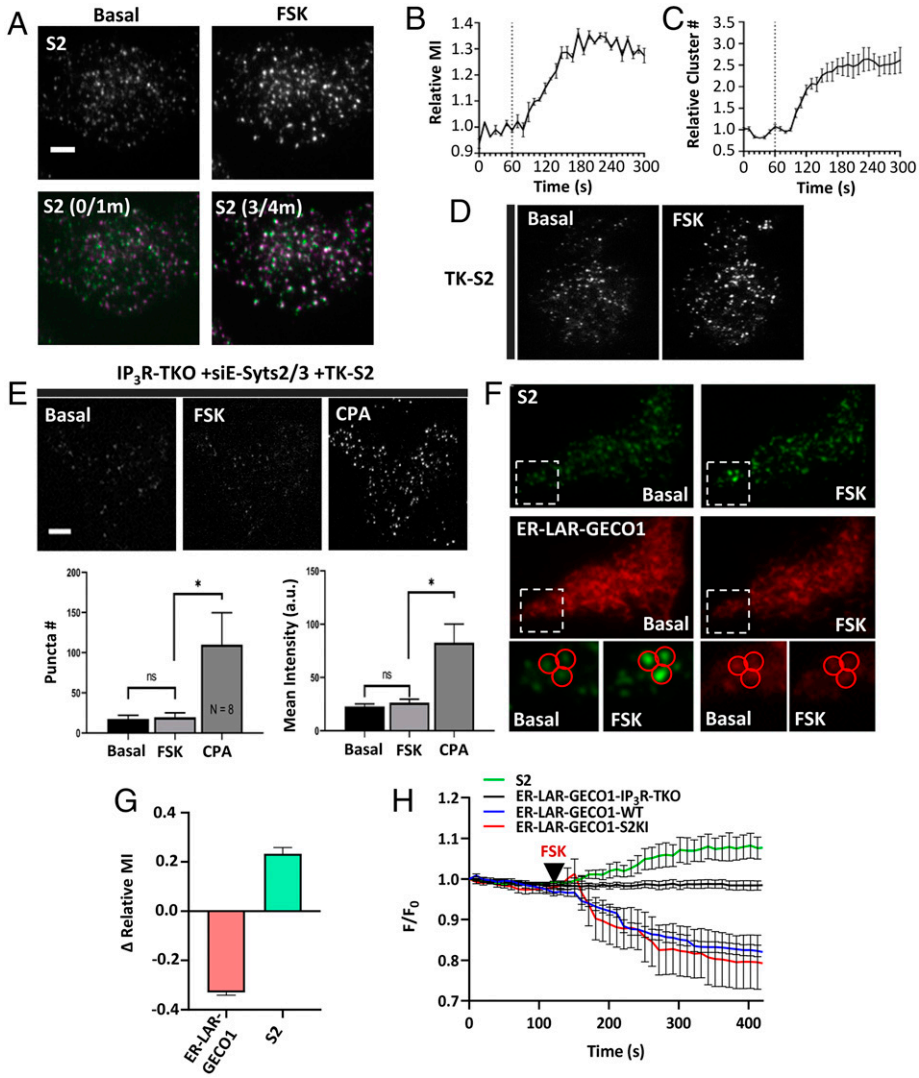

Fig. 5. STIM2 clustering is determined by IP_3R function. (*A*) mV-STIM2 (S2) clusters before and after 5 μM FSK stimulation (*Top*). Overlay images of mV-STIM2 at 0- and 1-min (0/1m) and 3- and 4-min (3/4m) time points (*Bottom*). (*B*) Increase of mV-STIM2 mean fluorescence intensity (MI) and relative number (cluster #) (*C*) in response to FSK treatment (added at 1-min time point, dotted line). (*D*) HEK293 cells expressing TK-YFP-STIM2 (TK-S2) before and after stimulation with FSK. (*E*) IP_3R-TKO cells (lack all three IP_3R subtypes), treated with siE-Syts2/3 and expressing TK-S2, before and after stimulation with 5 μM FSK and 25 μM CPA. Bar graphs showing number (puncta #) and mean intensity of TK-S2 clusters in the three conditions shown in the images ($n = 8$). Statistical tests were done using ANOVA with the significance presented as not significant (ns: $P > 0.05$) and significant (*$P < 0.05$). (*F*) STIM2-KI cells expressing ER-LAR-GECO1: S2 (*Top*) and ER-LAR-GECO1 (*Bottom*) under basal (unstimulated) and stimulated with FSK (5 μM). Enlargements of the region marked by a square are shown for visible camparisions. (*G*) Bar graph shows change in relative MI at the 5-min time point compared to basal (time point 1 min). Data are from three experiments and $n = 43$ immobile clusters). (*H*) Line graphs showing whole cell intensity of ER- LAR-GECO1 in WT, STIM2-KI (S2KI), and IP_3R-TKO cells, and S2 fluorescence only in S2KI expressing ER-LAR-GECO1. Addition of 5 μM FSK is indicated by the black arrows. All TIRFM images show representative cells from at least three experiments. (Scale bars, 5 μm.)

constructs of these chimeras were expressed in HEK cells. Although this STIM2 chimera (S1N-S2C) displayed preclustering in unstimulated cells, no immobile clusters were detected (Fig. 7*A*). In contrast, WT-STIM2 displayed robust preclustering with a population of immobile clusters (Fig. 7*B*, also see line scans *i* and *ii* from the two sets of cells). Additionally, a STIM1 chimera with STIM2 N terminus (S2N-S1C) displayed some preclusters with a few that were relatively immobile. The majority of S2N-S1C appeared to be tracking as was the case for WT-STIM1. There were no detectable clusters in cells expressing WT-STIM1 (Fig. 7 *C* and *D*).

Discussion

In the study described above, we utilized targeted gene editing to tag endogenous STIM2 with mVenus, which enabled us to study the distribution, dynamics, and regulation of the endogenous protein in unstimulated cells and after agonist stimulation. We show that endogenous STIM2 displays constitutive clustering within the subplasma membrane ER in resting cells under basal condition. Importantly, there is a small population of STIM2 clusters that is relatively immobile while the majority of them are mobile. Immobile STIM2 clusters are physiologically relevant as they are increased by agonist stimulation and contribute to initiation of SOCE in basal and agonist-stimulated cells. Importantly, we have identified critical cellular cues, which govern the clustering of STIM2 in cells under ambient conditions. Localization of STIM2 in the subplasma membrane ER is dependent on E-Syts2/3, which have been suggested to serve as constitutive tethers linking the ER with the PM (18). However, localization of ER in the subplasma membrane region of cells, or preexisting ER–PM

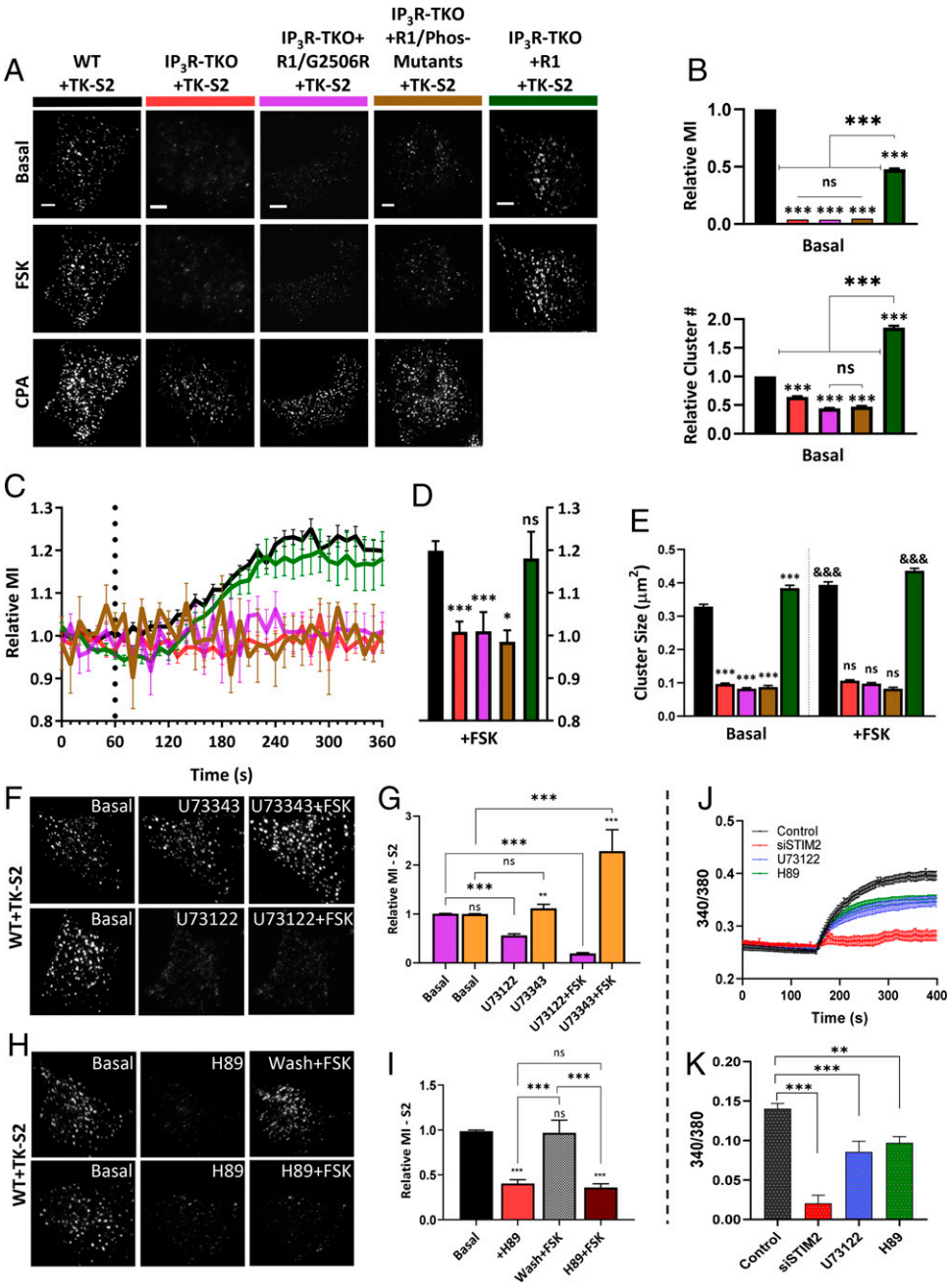

Fig. 6. STIM2 clustering is determined by IP_3R function. (*A*) HEK293 cells expressing TK-YFP-STIM2 (TK-S2): WT (black); IP_3Rs-TKO (lack all three IP_3R subtypes, red); IP_3R-TKO cells stably expressing a pore-dead mutant of IP_3R1 (IP_3R-TKO/G2506R, magenta); IP_3R-TKO cells expressing phosphorylation-deficient IP_3R1 with S1589A and S1755A mutations (IP_3R-TKO/Phos-mutants, brown); and IP_3R-TKO cells stably expressing IP_3R1 (IP_3R-TKO + IP_3R1, green), respectively, either unstimulated (basal) or consecutively stimulated with 5 μM FSK and 25 μM CPA. (*B*) Bar graphs show relative MI (*Top*) and relative number (*Bottom*) of TK-S2 clusters in basal condition for all cell types in *A*. (*C*) Time-dependent increases in relative MI of TK-S2 clusters calculated from cells shown in *A*. (*D*) Bar graphs show relative MI at the 5-min time point in *C*. (*E*) Bar graph showing relative size of TK-S2 clusters for the basal and FSK-treated cells in *A*. Basal values for all IP_3R-TKO cells were compared to WT, while FSK values for WT and all IP_3R-TKO cells were compared with their basal counterparts. (*F*) WT cells expressing TK-S2 showing clusters at basal (*Left*) and poststimulation with either 5 μM U73343 (inactive compound, *Middle*) and U73343 with 5 μM FSK (*Right*). *Bottom* set shows similar experiment done with the active PLC inhibitor, U73122 (5 μM). (*G*) Bar graphs showing relative MI at basal and after stimulation with compounds as indicated in *F*. (*H*) TK- S2 clusters in HEK293 cells under basal (*Left*), poststimulation with 5 μM H89 (*Middle*), and poststimulation with 5 μM FSK (*Right*). Treatment with FSK was either with a washout (wash) of H89 (*Top*) or without (*Bottom*). (*I*) Bar graphs showing relative MI at basal and after stimulation with compounds as indicated in *H*. Statistical tests were done using ANOVA with nonsignificant results presented ns: $P > 0.05$ and various levels of statistical significance as $^{*}P < 0.05$, $^{**}P < 0.01$, and $^{\&\&\&}/^{***}P < 0.001$. All TIRFM images show representative cells from at least three experiments. (Scale bars, 5 μm.) (*J*) Fura-2 fluorescence measurements presented as $F\text{-}F_0$ (mean ± SEM) of S2KI (control, black) and S2KI + siSTIM2 cells (red), S2KI + U73122 (blue), S2KI + H89 (green), treated with 1 mM CaCl (addition at 150s). (*K*) Bar graphs show change in $F\text{-}F_0$ due to 1 mM Ca^{2+} entry (four independent experiments with $n > 170$ cells).

junctions, is not sufficient for STIM2 preclustering. A major finding of this study is that IP_3R channel activity within subplasma membrane ER of cells underlies the constitutive clustering of STIM2. We show that immobile STIM2 clusters and immobile IP_3R are juxtaposed and localized in subplasma membrane ER. Functional immobile IP_3R in subplasma membrane ER are

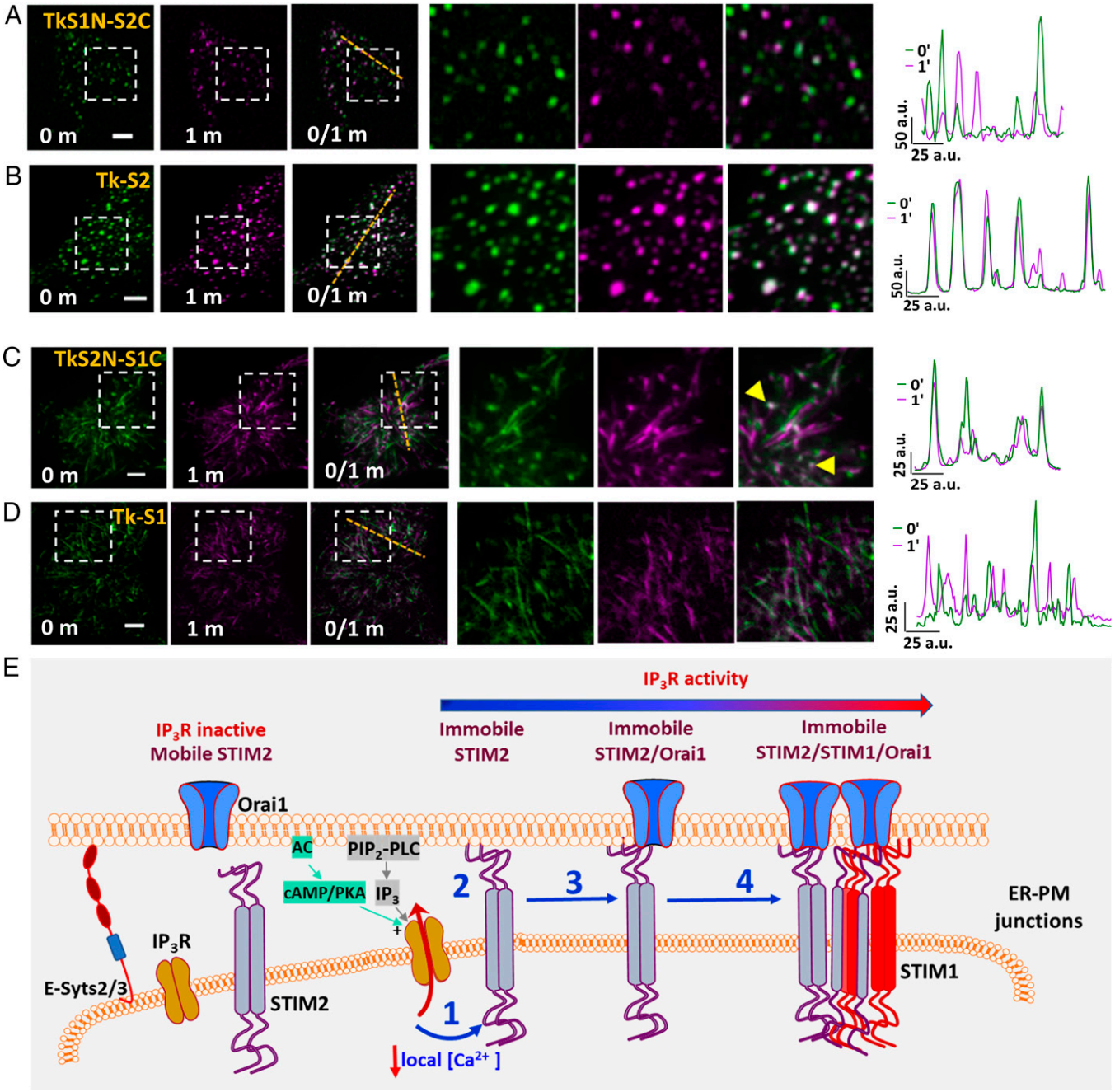

Fig. 7. STIM2 N terminus senses local $[Ca^{2+}]_{ER}$ decreases at subthreshold stimuli. HEK293 cells expressing (*A*) YFP-STIM2-STIM1N (STIM2 with STIM1 N terminus, S1N-S2C) or (*B*) YFP-STIM2 (control, S2-WT) in basal conditions (0- and 1-min time points individually and with overlay [0/1m]). Enlargement of demarcated region shown at *Right* and line scans (position shown in images). HEK293 cells expressing (*C*) YFP-STIM1-STIM2N (STIM1 with STIM2 N terminus, S2N-S1C) or (*D*) YFP-STIM1 (control, S1-WT) under basal conditions (0- and 1-min time points alone and with overlay [0/1m]). Enlargement of demarcated region shown in *Right* images and also line scans (position shown in images). All TIRFM images show representative cells from at least three experiments. (Scale bars, 5 μm.) a.u.: arbitrary units. (*E*) Proposed model: IP_3R and STIM2 are localized in the ER–PM junctional region. Under ambient conditions (without agonist addition), constitutive PLC-dependent PIP_2 hydrolysis as well as cAMP/PKA activity regulate IP_3R activity. When STIM2 is in the vicinity of a functional IP_3R, it senses the lower $[Ca^{2+}]_{ER}$ (1), which leads to scaffolding to the plasma membrane and immobilization (2). Orai1 is then recruited to immobile STIM2 (3) and with further $[Ca^{2+}]_{ER}$ decrease STIM1 is also recruited to immobile STIM2 (4). The model refers to cellular responses under ambient and low-intensity stimuli.

reported to rapidly sense and respond to increases in $[IP_3]$ generated by hydrolysis of plasma membrane PIP_2 (16). The close proximity of STIM2 and IP_3R clusters allows the luminal N terminus of STIM2 to sense a IP_3R-mediated decrease in local $[Ca^{2+}]_{ER}$, leading to immobilization of STIM2 in ER–PM junctions. Further, we also report that IP_3R activity in unstimulated cells is maintained by IP_3 that is generated by constitutive PLC-dependent PIP_2 hydrolysis. Unexpectedly, PKA inhibitors also caused a decrease in STIM2 preclustering, suggesting that cAMP/PKA signaling can also contribute to constitutive clustering of the protein. Consistent with this, addition of forskolin to cells increased the number of immobile STIM2 clusters in ER–PM junctional region. Together, these important findings reveal that regulation of IP_3R function under ambient conditions underlies

constitutive clustering of STIM2. We also infer that IP_3R activation under these conditions is likely to be transient, causing rapid local decrease in $[Ca^{2+}]_{ER}$ followed by refilling mediated by the SERCA pumps. In the absence of Ca^{2+} recycling in peripheral ER, e.g., in IP_3R-TKO cells, STIM2 preclustering in the ER–PM junctional region is suppressed. Similar suppression of immobile STIM2 clusters is seen when constitutive IP_3R activity is reduced by inhibition of PLC or PKA or when Ca^{2+} sensitivity of STIM2 N terminus is decreased. Conversely, preventing recycling by maximizing release enhances immobile clustering. Together, these findings reveal that continued recycling of Ca^{2+} in peripheral ER maintains constitutive clusters of STIM2 in the ER–PM junctional region, while sensing ER-Ca^{2+} store depletion causes immobilization of the protein.

We suggest that immobile STIM2 clusters represent the site of SOCE initiation in basal as well as agonist-stimulated conditions. These STIM2 clusters demarcate sites where Orai1 and STIM1 are recruited, which is especially relevant in cells under ambient conditions and following exposure to low-intensity stimuli. Use of a weak promoter to drive Orai1 expression allowed detection of a few immobile Orai1 clusters that are colocalized with immobile mV-STIM2 clusters even in unstimulated cells and increased following agonist stimulation. Our data indicate that the STIM2/Orai1 complex underlies basal Ca^{2+} entry in unstimulated cells since knockdown of endogenous STIM2 decreased basal Ca^{2+} entry as well as Orai1 clustering. In contrast, STIM1 clusters with immobile STIM2 only after agonist stimulation and prominent clustering is seen with longer stimulation times, i.e., with more depletion of $[Ca^{2+}]_{ER}$. Note that both Orai1 and STIM1 are stabilized within ER–PM junctions when coclustered with the relatively immobile STIM2, and the number of stable complexes are increased in a dose- and time-dependent manner after agonist stimulation. Thus, immobilization of STIM2 clusters in response to local $[Ca^{2+}]_{ER}$ decrease marks a critical checkpoint for SOCE initiation. This change in STIM2 clustering is also the first step in coupling ER-Ca^{2+} store depletion with SOCE activation. Close association between STIM1 and IP_3R is suggested to faciliate fast response of STIM1 to $[Ca^{2+}]_{ER}$ decrease following high-intensity stimuli (29). It is interesting to note that STIM2 complexes with RyR, STIM1, and Orai1 in T cells, contribute to generation of Ca^{2+} microdomains following T cell receptor stimulation (30). Conversely, Ca^{2+} binding N-terminal region of STIM proteins is suggested to suppress IP_3R function under resting conditions. This inhibition is relieved when STIMs are activated with increasing agonist concentrations (31). During the preparation of this manuscript, a mathematical model was described to explain the spontaneous Ca^{2+} microdomains that are detected in unstimulated T cells (32). According to this model, preformed clusters of STIM2/Orai1 are localized in close proximity to IP_3Rs, which facilitates STIM2 to detect reduction in local $[Ca^{2+}]_{ER}$ caused by spontaneous IP_3R activity. However, no experimental data were provided to support this model. The findings we report herein provide evidence that IP_3R activity in unstimulated cells is not spontaneous but rather that it is regulated by intracellular signals generated under ambient conditions. While further studies are required to determine the exact factors that govern localization of functional IP_3R near ER–PM junctions, our data reveal that STIM2 serves as the crucial first responder that senses the decrease in local ER-$[Ca^{2+}]$ mediated by IP_3Rs. This functional communication between IP_3R and STIM2 enables cells to distinguish between noise and a bona fide signal for activation of SOCE.

In conclusion, we have demonstrated here that preclustering of STIM2 in ER–PM junctions of unstimulated cells is not a random event but rather it is orchestrated by IP_3R function via decrease in local $[Ca^{2+}]_{ER}$, which is sensed by the STIM2 N terminus. Further, IP_3R activity, and therefore STIM2 preclustering, in cells in the absence of agonist stimulation is controlled by ambient PLC-dependent PM PIP_2 hydrolysis together with constitutive cAMP/PKA activity. As noted above, depending on the cell type, other factors that allosterically increase IP_3R activity can also act in a manner similar to PKA phosphorylation. We show that a small population of STIM2 clusters is immobilized within ER–PM junctions in response to decrease in local $[Ca^{2+}]_{ER}$ and this set of clusters likely represent the active state of STIM2. This is further illustrated in our model (Fig. 7*E*) that depicts STIM2 clusters localized in ER–PM junctional region together with IP_3R. When a mobile STIM2 cluster is in the vicinity of an activated "licensed" IP_3R, it senses the decrease in local $[Ca^{2+}]_{ER}$ and responds causing scaffolding of its C-terminal polybasic domain to PM PIP_2. This results in immobilization of the STIM2 cluster. Both Orai1 and STIM1 converge on these immobile STIM2 clusters and once coclustered with STIM2, these proteins also display decreased mobility. The relatively flexible C terminus of STIM2 (10, 33), as well as the lower Ca^{2+} affinity of its N-terminal EF-hand domain (4), together with the juxtaposition of IP_3R in the ER–PM junctional region, allows it to sense and rapidly respond to decreases in local $[Ca^{2+}]_{ER}$. This critical functional link between IP_3R and STIM2 underlies the constitutive clustering of STIM2 and ensures the coupling of ER-Ca^{2+} store release events with activation of SOCE and regulation of Ca^{2+} signaling in the cell.

Materials and Methods

Cell Culture, Plasmids, RNAi Transfection, and Reagents. HEK293 cells were maintained and transfected with various siRNAs or plasmids as described in *SI Appendix*.

Knockin of mVenus in STIM2 Gene. The standard method for CRISPR/Cas9 based approach was followed to knockin the mVenus tag at STIM2 N terminus. Details of the method including that for cell sorting and establishing a single-cell clonal line are provided in *SI Appendix*.

Cellular Imaging and Image Analysis. $[Ca^{2+}]_i$ imaging measurements, confocal microscopy, ZEISS AiryScan, and TIRF microscopy (TIRFM) were all used for live-cell imaging experiments described in the text and figure legends (details of microscope, acquisition, and image analysis are provided in *SI Appendix*).

Statistics. Data analysis was performed using Origin (OriginLab Corporation) and GraphPad (GraphPad Software). Statistical comparisons between two groups were made using Student's *t* test, whereas comparisons of multiple groups were made using ANOVA followed by Sidak multiple comparisons test. Statistical significance was shown as significant at $*P < 0.05$, $**P < 0.01$ and $***P < 0.001$, or nonsignificant at $P > 0.05$ (ns).

Data Availability. All study data are included in the article and/or *SI Appendix*.

ACKNOWLEDGMENTS. We thank Dr. Tamas Balla (Eunice Kennedy Shriver National Institute of Child Health and Human Development, NIH) for Orai1-LL-CFP; Dr. Tobias Meyer (Stanford University) for YFP-STIM2; Dr. Richard Lewis (Stanford University) for mCherry-STIM1; and Dr. Jen Liou (University of Texas Southwestern Medical Center) for GFP-MAPPER. We also thank Elina Stregevsky, Mehrnoosh Abshari, Luxia Zhang, and George McGrady (National Institute of Dental and Craniofacial Research [NIDCR] Combined Technical Research Core) for help in cell sorting and DNA sequencing. Funding for this work was provided by NIDCR-Division of Intramural Research, NIH (Z01-DE00438-33) to I.A. and NIH grants R35-HL150778 to M.T. and R01 DE019245 to D.I.Y.

1. M. Prakriya, R. S. Lewis, Store-operated calcium channels. *Physiol. Rev.* **95**, 1383–1436 (2015).
2. H. L. Ong, K. P. Subedi, G. Y. Son, X. Liu, I. S. Ambudkar, Tuning store-operated calcium entry to modulate Ca^{2+}-dependent physiological processes. *Biochim. Biophys. Acta Mol. Cell Res.* **1866**, 1037–1045 (2019).
3. J. Liou, M. Fivaz, T. Inoue, T. Meyer, Live-cell imaging reveals sequential oligomerization and local plasma membrane targeting of stromal interaction molecule 1 after Ca^{2+} store depletion. *Proc. Natl. Acad. Sci. U.S.A.* **104**, 9301–9306 (2007).
4. O. Brandman, J. Liou, W. S. Park, T. Meyer, STIM2 is a feedback regulator that stabilizes basal cytosolic and endoplasmic reticulum Ca^{2+} levels. *Cell* **131**, 1327–1339 (2007).

5. J. Liou *et al.*, STIM is a Ca2+ sensor essential for Ca^{2+}-store-depletion-triggered Ca^{2+} influx. *Curr. Biol.* **15**, 1235–1241 (2005).
6. M. Prakriya *et al.*, Orai1 is an essential pore subunit of the CRAC channel. *Nature* **443**, 230–233 (2006).
7. M. Vig *et al.*, CRACM1 multimers form the ion-selective pore of the CRAC channel. *Curr. Biol.* **16**, 2073–2079 (2006).
8. A. V. Yeromin *et al.*, Molecular identification of the CRAC channel by altered ion selectivity in a mutant of Orai. *Nature* **443**, 226–229 (2006).
9. H. L. Ong *et al.*, STIM2 enhances receptor-stimulated Ca^{2+} signaling by promoting recruitment of STIM1 to the endoplasmic reticulum-plasma membrane junctions. *Sci. Signal.* **8**, ra3 (2015).
10. K. P. Subedi, H. L. Ong, G. Y. Son, X. Liu, I. S. Ambudkar, STIM2 induces activated conformation of STIM1 to control Orai1 function in ER-PM junctions. *Cell Rep.* **23**, 522–534 (2018).
11. A. Berna-Erro, I. Jardin, G. M. Salido, J. A. Rosado, Role of STIM2 in cell function and physiopathology. *J. Physiol.* **595**, 3111–3128 (2017).
12. X. Wang *et al.*, Distinct Orai-coupling domains in STIM1 and STIM2 define the Orai-activating site. *Nat. Commun.* **5**, 1–11 (2014).
13. A. M. Miederer *et al.*, A STIM2 splice variant negatively regulates store-operated calcium entry. *Nat. Commun.* **6**, 1–12 (2015).
14. C. L. Chang *et al.*, Feedback regulation of receptor-induced Ca^{2+} signaling mediated by E-Syt1 and Nir2 at endoplasmic reticulum-plasma membrane junctions. *Cell Rep.* **5**, 813–825 (2013).
15. M. M. Wu, E. D. Covington, R. S. Lewis, Single-molecule analysis of diffusion and trapping of STIM1 and Orai1 at endoplasmic reticulum-plasma membrane junctions. *Mol. Biol. Cell* **25**, 3672–3685 (2014).
16. N. B. Thillaiappan, A. P. Chavda, S. C. Tovey, D. L. Prole, C. W. Taylor, Ca^{2+} signals initiate at immobile IP_3 receptors adjacent to ER-plasma membrane junctions. *Nat. Commun.* **8**, 1–16 (2017).
17. M. K. Korzeniowski, I. M. Manjarrés, P. Varnai, T. Balla, Activation of STIM1-Orai1 involves an intramolecular switching mechanism. *Sci. Signal.* **3**, ra82 (2010).
18. F. Giordano *et al.*, $PI(4,5)P_{(2)}$-dependent and $Ca^{(2+)}$-regulated ER-PM interactions mediated by the extended synaptotagmins. *Cell* **153**, 1494–1509 (2013).
19. O. Idevall-Hagren, A. Lü, B. Xie, P. De Camilli, Triggered Ca^{2+} influx is required for extended synaptotagmin 1-induced ER-plasma membrane tethering. *EMBO J.* **34**, 2291–2305 (2015).
20. Y. J. Chen, C. G. Quintanilla, J. Liou, Recent insights into mammalian ER-PM junctions. *Curr. Opin. Cell Biol.* **57**, 99–105 (2019).
21. L. E. Wagner, 2nd, S. K. Joseph, D. I. Yule, Regulation of single inositol 1,4,5-trisphosphate receptor channel activity by protein kinase A phosphorylation. *J. Physiol.* **586**, 3577–3596 (2008).
22. D. I. Yule, M. J. Betzenhauser, S. K. Joseph, Linking structure to function: Recent lessons from inositol 1,4,5-trisphosphate receptor mutagenesis. *Cell Calcium* **47**, 469–479 (2010).
23. K. J. Alzayady *et al.*, Defining the stoichiometry of inositol 1,4,5-trisphosphate binding required to initiate Ca^{2+} release. *Sci. Signal.* **9**, ra35 (2016).
24. L. E. Terry, K. J. Alzayady, A. M. Wahl, S. Malik, D. I. Yule, Disease-associated mutations in inositol 1,4,5-trisphosphate receptor subunits impair channel function. *J. Biol. Chem.* **295**, 18160–18178 (2020).
25. L. E. Wagner, 2nd, W. H. Li, S. K. Joseph, D. I. Yule, Functional consequences of phosphomimetic mutations at key cAMP-dependent protein kinase phosphorylation sites in the type 1 inositol 1,4,5-trisphosphate receptor. *J. Biol. Chem.* **279**, 46242–46252 (2004).
26. O. Mignen, J. L. Thompson, T. J. Shuttleworth, Arachidonate-regulated Ca^{2+}-selective (ARC) channel activity is modulated by phosphorylation and involves an A-kinase anchoring protein. *J. Physiol.* **567**, 787–798 (2005).
27. M. J. Betzenhauser *et al.*, ATP modulation of Ca2+ release by type-2 and type-3 inositol (1, 4, 5)-triphosphate receptors. Differing ATP sensitivities and molecular determinants of action. *J. Biol. Chem.* **283**, 21579–21587 (2008).
28. D. L. Prole, C. W. Taylor, Inositol 1,4,5-trisphosphate receptors and their protein partners as signalling hubs. *J. Physiol.* **594**, 2849–2866 (2016).
29. A. Sampieri, K. Santoyo, A. Asanov, L. Vaca, Association of the IP3R to STIM1 provides a reduced intraluminal calcium microenvironment, resulting in enhanced store-operated calcium entry. *Sci. Rep.* **8**, 1–13 (2018).
30. B. P. Diercks *et al.*, ORAI1, STIM1/2, and RYR1 shape subsecond Ca^{2+} microdomains upon T cell activation. *Sci. Signal.* **11**, 1–13 (2018).
31. S. M. Emrich *et al.*, Omnitemporal choreographies of all five STIM/Orai and IP_3Rs underlie the complexity of mammalian Ca^{2+} signaling. *Cell Rep.* **34**, 108760 (2021).
32. D. Gil, A. H. Guse, G. Dupont, Three-dimensional model of sub-plasmalemmal Ca^{2+} microdomains evoked by the interplay between ORAI1 and $InsP_3$ receptors. *Front. Immunol.* **12**, 659790 (2021).
33. S. M. Emrich *et al.*, Cross-talk between N-terminal and C-terminal domains in stromal interaction molecule 2 (STIM2) determines enhanced STIM2 sensitivity. *J. Biol. Chem.* **294**, 6318–6332 (2019).